Large enhancement of fully resonant sum-frequency generation through quantum control via continuum states

A. K. Popov,[1,2,*] V. V. Kimberg,[2,†] and Thomas F. George[3,‡]
[1]*Department of Physics & Astronomy and Department of Chemistry, University of Wisconsin–Stevens Point, Stevens Point, Wisconsin 54481, USA*
[2]*Institute of Physics of the Russian Academy of Sciences, 660036 Krasnoyarsk, Russia*
[3]*Department of Chemistry & Biochemisty and Department of Physics & Astronomy, University of Missouri–St. Louis, St. Louis, Missouri 63121, USA*
(Received 14 March 2003; published 21 April 2004)

A theory of quantum control of short-wavelength sum-frequency generation, which employs the continuum states, is developed. The proposed scheme employs all-resonant coupling and trade-off optimization of the accompanying constructive and destructive quantum interference effects in the lower-order and higher-order polarizations controlled by the overlap of two autoionizinglike laser-induced continuum structures. The scheme does not rely on adiabatic passage, coherent population trapping or maximum atomic coherence as a means to facilitate maximum output. The opportunities for manipulating transparency of the medium and refractive index for the fundamental and generated radiations, as well as nonlinear polarization in the multiple-resonant medium, are shown. This opens the feasibility of creating frequency-tunable narrowband filters, polarization rotators, and dispersive elements for vacuum ultraviolet radiation. The features specific for quantum interference in Doppler-broadened media are investigated. The feasibility of almost complete conversion of long-wavelength fundamental radiation into generated short-wavelength radiation, and of a dramatic decrease in the intensity of required fundamental radiations, is shown.

DOI: 10.1103/PhysRevA.69.043816 PACS number(s): 42.50.Gy, 42.65.Ky, 32.80.Fb, 32.80.Qk

I. INTRODUCTION

The fact that two resonant intra-atomic oscillations (quantum pathways) may interfere has been understood and employed in nonlinear spectroscopy since the widespread use of lasers began. In the example of a three-level scheme, one of two such oscillations can be produced by resonant probe radiation and another by the same probe radiation in cooperation with an auxiliary field applied to the adjacent transition. Such oscillations may suppress (destructive interference) or enhance (constructive interference) each other, enabling one to eliminate or alternatively enhance the coupling of light and matter. The relative phases and amplitudes of such oscillations can be varied by changing the resonance detuning and strength of the auxiliary control field. Since such nonlinear interference effects (NIE) [1–6] are inherent to various resonantly enhanced nonlinear interactions of light and atoms, NIE-based feasibilities for producing laser-induced transparency or, alternatively, new absorption and emission peaks, as well as manipulating their position and spectral lineshape, were consequently predicted and observed. A classification of various possible NIE and conditions for their separate observation were discussed in Refs. [3,5,6]. In many early experiments, near-resonance coupling of high-power ruby laser radiation with two excited states of potassium atom was employed. In combination with the Stokes component of stimulated Raman emission in nitrobenzene, this enabled the monitoring of a two-photon ladder-type resonance with the ground state of the atom accompanied by an intermediate one-photon resonance. A variety of proof-of-principle experiments on NIE, including four- and multiwave mixing, were performed [7]. Other options were provided by the resonance interaction of He-Ne lasers and Ne atoms excited in a discharge. Thus the NIE-based opportunity for manipulating optical properties of the resonance media from enhanced absorption to amplification without population inversion via entire transparency were discussed in detail and numerically illustrated for the example of the Ne atom driven by He-Ne laser [6,8]. A review of the relevant early theoretical and experimental work was given in Ref. [9].

Resonant nonlinear optics, and specifically four-wave mixing (FWM), in atomic gases have enjoyed tremendous developments over recent years in connection with the concepts of electromagnetically induced transparency, coherent population trapping, and maximum coherence achievable between the discrete states [10–14]. Coherent population trapping and maximum coherence usually imply utilization of Raman-type coupling with metastable states or light pulses shorter than the shortest relaxation rate in the gas. Manipulating FWM with the control field in a more complex five-level scheme has recently been investigated in Ref. [15].

So far a great majority of papers has dealt with resonant schemes predominantly composed by discrete levels, especially with regards to the FWM processes. Quantum interference is usually employed for a decrease of lower-order (ab-

*Electronic address: apopov@uwsp.edu
†Present address: Theoretical Chemistry, Department of Biotechnology, SCFAB Roslargstullbacken, 15 Royal Institute of Technology (KTH), S-106 91 Stockholm, Sweden. Electronic address: viktor@theochem.kth.se
‡Electronic address: tfgeorge@umsl.edu

sorptive and dispersive) susceptibilities, whereas higher-order (generating) nonlinear polarization is increased. Basically, such an approach requires two-photon coupling mediated by one-photon resonance for fundamental and often for generated radiations. The claimed primary implementation of such studies is to extend the generated radiation to the vacuum ultraviolet (vuv) wavelength range where the efficiency to be achieved exceeds that in crystals. However, energy levels of atoms and molecules are fundamentally nonequidistant and converge swiftly to the photoionization limit. Therefore, the coupling of the generated vuv and at least one of the fundamental radiations with the continuous energy states becomes almost inevitable. This makes an understanding of FWM and other accompanying nonlinear-optical processes associated with continuum states and the investigation of the feasibilities of their quantum control and enhancement of basic and practical importance.

For a long time, the continuum of quantum states, such as that observed in the ionization of an atom or dissociation of a molecule, was regarded as an incoherent dissipation medium. This changed with studies [16–18] that proposed that the optical properties determined by quantum transitions to the continuum can be manipulated with control lasers in the same manner as the NIE associated with the discrete states. Thus opportunities were predicted for the formation of narrow resonances embedded in an otherwise unstructured continuum. The shape of such spectral structures is similar to that of a real autoionizing (Fano) resonance [19], but their position, strength, and even their profile can be manipulated with a control laser. Due to the interference origin, the features of such autoionizinglike laser-induced continuum structures (LICS) were found to be different in absorption, refraction, ionization (dissociation), and FWM susceptibilities [18,20,21]. In particular, the opportunity of producing a transparency window for the generated radiation without a substantial decrease of the FWM polarization was proposed in Ref. [18]. Since the first proof-of-principle experiments [22], where such induced resonances were observed in the refractive index associated with the transition from the ground state to the ionization continuum of atomic cesium, great progress has been made in developing a deeper understanding of quantum coherence and related laser-induced processes associated with continuum states [23]. The experiments have confirmed the key predictions based on the simplified theoretical models, although in some cases discrepancies have been revealed. Main efforts have been applied to the investigation of LICS-controlled polarization rotation and photoionization, often in the vicinity of real autoionizing states. Only very few publications have dealt with LICS-type FWM schemes [24], but for all these, the specific features attributed to coupling with the strong fields mediated by one-photon resonance have not been investigated so far. The appearance and consequences of quantum coherence and interference processes are very different in the cw regime, where relaxation processes play a crucial role, compared to the pulsed regime of rapid adiabatic passage. Nor have the features attributed to either the cw resonant FWM coupling or the coupling with inhomogeneously broadened transitions, been properly addressed in the context of LICS-based quantum control. Most of the recent work on the coherent coupling via the continuum deal with the suppression of ionization and adiabatic passage between two discrete excited metastable levels via ionization continuum in Raman-like Λ-schemes driven by properly ordered laser pulses [25,26].

This paper is aimed at filling the outlined gaps. It proposes a scheme that combines the advantages of the all-resonant enhancement of the short-wavelength sum-frequency FWM response of the medium and LICS-based coherent quantum control. This is shown to enable one to decrease the required intensities of the applied fields down to those characteristic for cw radiation. Consequently, the scheme specifically addresses the cases, where neither the coherent population trapping nor the maximum coherence can be achieved. Hence, it does not rely on such processes. Besides, it offers great manipulating flexibility through a suggested employment of several variable strong fields and, at the same time, avoids the effects associated with the population transfer, ionization, and depletion of the resonant atoms. It is shown that the resonant interaction of several strong fields gives rise to qualitatively different effects compared to the previously studied schemes where all fundamental radiations are imperturbatively weak and only one control field is strong. The combined influence of the interference of two LICS on the laser-induced transparency and dispersion for both fundamental and generated radiations, as well as on the modification of FWM polarization, is studied. The effect of inhomogeneous (Doppler) broadening of the coupled transition on the appearance of NIE in the LICS-assisted schemes is investigated. The latter includes anisotropic spectra and narrow sub-Doppler spectral structures. The optical properties of the materials in the vicinity of discrete transitions are shown to also be manipulated through the interference of two LICS that provide a considerably different appearance compared to quantum control in a solely discrete scheme. The dependence of NIE on the distribution of the oscillation strengths over the continuum is shown to be of critical importance. Corresponding experiments may give information about complex Fano parameters attributed to the excited discrete states and the continuum, which are, so far, less known. However, the primary goal of the paper is the implementation of the outlined effects for control over the evolution of the generated and fundamental radiation along the otherwise strongly absorbing media. The factors discriminating the most favorable regimes of generation are determined. They suggest the feasibilities of almost complete conversion of long-wavelength fundamental radiation into short-wavelength generated output under an appreciably reduced intensity of the fundamental radiations. Such opportunities are shown feasible through a trade-off analysis of the accompanying interference effects in the lower-order and higher-order polarizations. An appropriate adjustment of the overlap of two LICS that ensures the effect is proposed to be achievable with the control field, which does not contribute directly to four-wave mixing. Such opportunities are demonstrated through numerical simulations that employ the typical atomic parameters.

This paper is organized as follows. In the next section we discuss the discriminating parameters, which determine frequency conversion in a resonant absorbing medium, and outline the calculational procedures. Section III presents the

density-matrix equations and their solutions, which describe local optical characteristics of the resonant medium driven by several strong fields. Laser-induced structures in discrete and continuous spectra of absorption and refraction are investigated in Sec. IV. Section V considers specific features of absorption and dispersive spectra at Doppler-broadened transitions. Resonance sum-frequency generation in strongly absorbing media controlled by the interference of two LICS is studied in Sec. VI. The main outcomes of the work are summarized in Sec. VII.

II. FREQUENCY CONVERSION IN ABSORBING MEDIA: DISCRIMINATING PARAMETERS

A maximum achievable conversion efficiency and corresponding medium length are determined by the interplay of concomitant NIE-based changes in absorption, refraction, and FWM polarization. In this section we show that the specific qualitatively different generation regimes may develop under such conditions. The microscopic parameters will be derived to be used and analyzed in the following sections for the investigation of the spectral properties of resonant sum-frequency generation in optically dense media. Consequently, let us consider four plane-polarized electromagnetic waves traveling along the z axis of an isotropic medium,

$$E^j(z,t) = \mathrm{Re}\{E_j(z)\exp[i(\omega_j t - k_j z)]\}, \tag{1}$$

where k_j is the complex wave number corresponding to the frequency ω_j $(j=1,2,3,S)$ that accounts for depletion along the medium. We assume that the fields E_1 and E_S are weak compared to the driving fields E_2 and E_3, which do not vary along the medium. On the contrary, the fields E_1 and E_S may change considerably along the medium because of absorption and nonlinear-optical conversion. Then the spatial behavior of the waves E_S and E_1 is given by two coupled reduced wave equations,

$$\begin{aligned} dE_S(z)/dz &= i2\pi k'_S \chi_S^{(3)} E_2 E_3 E_1(z)\exp(i\Delta k z), \\ dE_1(z)/dz &= i2\pi k'_1 \chi_1^{(3)} E_2^* E_3^* E_S(z)\exp(-i\Delta k z). \end{aligned} \tag{2}$$

Here, $k_j = k'_j - ik''_j = (2\pi\omega_j/c)\chi_j$, $k''_j = \alpha_j/2$; χ_j, α_j are the effective linear susceptibilities and absorption indices for the corresponding radiations; and $\chi_1^{(3)}, \chi_S^{(3)}$ are the FWM nonlinear susceptibilities: $\omega_S \leftrightarrow \omega_1+\omega_2+\omega_3$, $\Delta k = k_S - k_1 - k_2 - k_3$. The quantum conversion efficiency of the radiation E_1 into E_S that varies along the medium is defined by the equation

$$\eta_\mathrm{q} = \frac{k'_1}{k'_S}\left|\frac{E^S(t,z)}{E_1(0)}\right|^2 = \frac{k'_1}{k'_S}\left|\frac{E_S(z)}{E_1(0)}\right|^2 \exp(-\alpha_S z). \tag{3}$$

Let us first consider the case of low conversion efficiency, for which the change in the E_1 caused by the nonlinear-optical conversion can be ignored. Then the second equation in (2) can be ignored as well and, with account of the boundary condition $E_S(z=0)=0$, one obtains the following equations:

$$E_S(z) = (2\pi k'_S/\Delta k)\chi_S^{(3)} E_1 E_2 E_3[\exp(-i\Delta k z) - 1], \tag{4}$$

$$\eta_\mathrm{q}(z) = (k'_S k'_1/|\Delta k|^2)|2\pi\chi_S^{(3)} E_2 E_3|^2 \exp(-\alpha_S z)|\exp(-i\Delta k z) - 1|^2. \tag{5}$$

If the medium length is much shorter than the minimum absorption length $L_{abs} = \min\{L_1 = 2/\alpha_1, L_S = 2/\alpha_S\}$ and both of these are assumed much shorter than the coherence length $L_{coh} = \Delta k'^{-1}$, then Eq. (5) reduces to the approximate formula

$$\eta_q = k'_S k'_1 |2\pi\chi_S^{(3)} E_2 E_3|^2 L_\mathrm{e}^2, \tag{6}$$

where L_e presents either the length of the medium (in the case of weak absorption) or the optimal length of the order of $\min\{L_{abs}, L_{coh}\}$.

Alternatively, assume that phase mismatch, which includes the nonlinear contribution, is compensated by the standard technique, e.g., with a buffer gas. This is feasible in the scheme under investigation, because all the driving fields are homogeneous along the medium. Then for the more general and complex case of considerable conversion and a medium with substantial absorption dispersion $(\alpha_1 \neq \alpha_S)$, but $\Delta k' = 0$, the solution of Eqs. (2) takes the form [27]

$$\eta_q(z) = 4(\tilde{\eta}_{q0}/|b|)\exp[-(\alpha_1+\alpha_S)z/2] \times \left[\sinh^2\left(\sqrt{\frac{|b|-b}{2}}\frac{z}{2}\right) + \sin^2\left(\sqrt{\frac{|b|+b}{2}}\frac{z}{2}\right)\right]. \tag{7}$$

Here,

$$\tilde{\eta}_{q0} = k'_1 k'_S |2\pi\chi_S^{(3)} E_2 E_3|^2, \quad b = 4\tilde{\eta}_{q0} - (\alpha_1 - \alpha_S)^2/4, \tag{8}$$

and the relationship $\chi_1^{(3)*} = \chi_S^{(3)}$ is assumed. According to (6), $\tilde{\eta}_{q0}$ identifies the local conversion rate (efficiency per unit of the medium length under negligible depletion of the radiations). Parameter b defines the difference between the rates of nonlinear-optical conversion and dispersion of absorption of the radiations. This difference is usually determined by the larger of the indices. If $b>0$, the conversion rate of photons $\hbar\omega_1$ into $\hbar\omega_S$ exceeds the absorption rate; if $b=0$, the rates are equal; and if $b<0$, the conversion rate is less than the absorption rate. Consequently, Eq. (7) predicts three qualitatively different evolutions of the generated radiation along the medium:

$$\eta_q(z) = (4\tilde{\eta}_{q0}/b)\exp\{-(\alpha_1+\alpha_S)z/2\} \times \sin^2(\sqrt{b}z/2), \quad \text{at } b>0, \tag{9a}$$

$$\eta_q(z) = \tilde{\eta}_{q0} z^2 \exp\{-(\alpha_1+\alpha_S)z/2\}, \quad \text{at } b=0, \tag{9b}$$

$$\eta_q(z) = (4\tilde{\eta}_{q0}/|b|)\exp\{-(\alpha_1+\alpha_S)z/2\} \times \sinh^2(\sqrt{|b|}z/2), \quad \text{at } b<0. \tag{9c}$$

The first Eq. (9a) presents a damping oscillatory dependence of the transfer of the weak radiations from one to another and back along the medium, where each succedent maximum is smaller than the previous one. The other two equations, (9b) and (9c), describe the plots with one maximum, which is

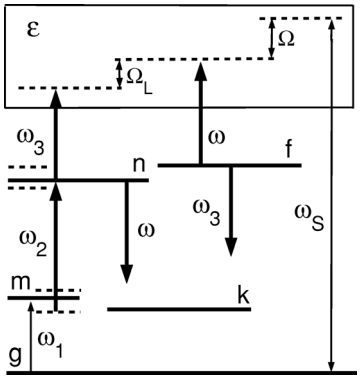

FIG. 1. LICS-based coherent quantum control in ladder schemes.

achievable over larger optical densities $(\alpha_1+\alpha_S)z$ and reaches a greater magnitude in the case (9b). Since the local conversion and absorption rates are interrelated, the factor b is the most important discrimination parameter to be optimized in order to achieve a maximum conversion efficiency under the given experimental conditions.

The susceptibilities $\chi_S^{(3)}$, $\chi_1^{(3)}$, χ_S, and χ_1 are derived from the medium polarizations at the corresponding frequencies:

$$P(\omega_j)=\chi_j E_j,$$
$$P^{\mathrm{NL}}(\omega_S)=\chi_S^{(3)}E_1E_2E_3, \quad P^{\mathrm{NL}}(\omega_1)=\chi_1^{(3)}E_SE_2^*E_3^*. \tag{10}$$

Traveling polarization waves are calculated conveniently with the aid of a density matrix, ρ_{ij}, as

$$\mathcal{P}(\omega_j)=N\rho_{ij}(\omega_j)d_{ji}+\text{c.c.}, \tag{11}$$

where N is the atomic number density in the medium, and d_{ji} is a matrix element of the projection of the transition electric-dipole moment along the direction of the electric vector of the corresponding field. Thus, the problem under consideration reduces to calculating the off-diagonal elements of the density matrix.

III. DENSITY MATRIX MASTER EQUATIONS AND THEIR SOLUTIONS

Let us consider the transition scheme depicted in Fig. 1. A strong field E_2 at frequency ω_2 is close to resonance with the transition between levels m and n, while the other strong fields E_3 and E at frequencies ω_3 and ω may couple levels n and f with the same states in the continuum. The field E_1 at ω_1 is close to resonance with the transition from the ground state to level m, and E_S at the frequency ω_S couples the ground state to the state belonging to the continuum. These radiations are assumed to be nonperturbative, so that one can disregard a depletion of atoms caused by photoionization and by a change in the level populations due to the all-resonant couplings. Radiation at ω_S can be either a probe or generated through four-wave mixing, depending on whether another weak field at ω_1 is turned on. Consequently, we shall investigate two different problems. One is the LICS-based coherent control of absorption and refractive indices at ω_1 and ω_S, when both are independent probe radiations. Potential applications include frequency-tunable narrow-band filters, dispersive elements, and polarization rotators in short-wavelength ranges, where competitive materials otherwise are not available. Another problem concerns the optimization of short-wavelength generation in an initially optically thick (i.e., strongly absorbing) medium driven by several strong fields, while the indicated frequencies are locked as $\omega_S=\omega_1+\omega_2+\omega_3$, and bound-free atomic transitions play an important role. A variable control field E plays a key role in optimization of the interplay of NIE in absorption, phase matching, and FWM coupling. The frequency of this field is tuned in such a way that it couples an empty level f with the same continuum states that are coupled with any other fields. Thus this field opens and manipulates a supplementary interfering set of quantum pathways. Actually, the nearby red- and blue-shifted continuum states may also contribute to interference, some in a constructive, others in a destructive way. The overall result is given by integration over all such states. Besides continuum states, a variety of other off-resonant discrete states, which are represented by level k in Fig. 1, may contribute as well to the supplementary quantum pathways turned on by the control field E. Basically, the sum over the contribution of all such states must be taken along with the integration over continuum states. It is supposed that the detunings $|\omega_1-\omega_{gm}|$, $|\omega_1+\omega_2-\omega_{gn}|$, and $|\omega-\omega_3-\omega_{nf}|$ are considerably less than all the other detunings, which validates the employed approximation of overall resonant or quasiresonant coupling.

The equations for the density matrix, considered in the interaction representation within first order in weak fields of the perturbation theory, can be written as follows:

$$d\rho_{gm}/dt+\Gamma_{gm}\rho_{gm}=i(\rho_{gg}V_{gm}+\rho_{gn}V_{nm}),$$
$$d\rho_{gn}/dt+\Gamma_{gn}\rho_{gn}=i\int\rho_{g\varepsilon}V_{\varepsilon n}d\varepsilon+i\rho_{gm}V_{mn}+i\sum\rho_{gk}V_{kn},$$
$$d\rho_{gf}/dt+\Gamma_{gf}\rho_{gf}=i\int\rho_{g\varepsilon}V_{\varepsilon f}d\varepsilon+i\sum\rho_{gk}V_{kf}, \tag{12}$$
$$d\rho_{g\varepsilon}/dt=i(\rho_{gg}V_{g\varepsilon}+\rho_{gn}V_{n\varepsilon}+\rho_{gf}V_{f\varepsilon}),$$
$$d\rho_{gk}/dt+\Gamma_{gk}\rho_{gk}=i(\rho_{gn}V_{nk}+\rho_{gf}V_{fk}).$$

Here, the index ε denotes the continuum states; $V_{mn}=G_{mn}\exp[i(\omega_2-\omega_{nm})t]$, $V_{g\varepsilon}=G_{g\varepsilon}\exp[i(\omega_S-\omega_{g\varepsilon})t]$, $V_{n\varepsilon}=G_{n\varepsilon}\exp[i(\omega_3-\omega_{n\varepsilon})t]$, $V_{gm}=G_{gm}\exp[i(\omega_1-\omega_{gm})t]$, $V_{f\varepsilon}=G_{f\varepsilon}\exp[i(\omega-\omega_{f\varepsilon})t]$, $V_{kn}=G_{kn}\exp[i(\omega-\omega_{kn})t]$ and $V_{kf}=G_{kf}\exp[i(\omega_3-\omega_{kf})t]$ are the matrix elements of the Hermitian interaction Hamiltonian $\hat{V}$, considered in the electric-dipole approximation and in the interaction representation (in units of $\hbar$); $V_{ij}=V_{ji}^*$; $G_{mn}=-E_2d_{mn}/2\hbar$, $G_{g\varepsilon}=-E_4d_{g\varepsilon}/2\hbar$, etc.; and Γ_{ij} is the homogeneous halfwidth of the ij transition (see Fig. 1). In the approximation of the weak fields E_1 and E_S, we obtain $\rho_{gg}=1$, $\rho_m=\rho_n=\rho_f=0$.

Under steady-state conditions, each off-diagonal element of the density matrix is a sum of two components, which may oscillate at different frequencies:

$$\rho_{g\varepsilon} = r_{g\varepsilon}\exp[i(\omega_S-\omega_{g\varepsilon})t] + R_{g\varepsilon}\exp[i(\omega_1+\omega_2+\omega_3-\omega_{g\varepsilon})t],$$

$$\rho_{gn} = r_{gn}\exp[i(\omega_S-\omega_3-\omega_{gn})t] + R_{gn}\exp[i(\omega_1+\omega_2-\omega_{gn})t],$$

$$\rho_{gm} = r_{gm}\exp[i(\omega_S-\omega_3-\omega_2-\omega_{gm})t] + R_{gm}\exp[i(\omega_1-\omega_{gm})t], \tag{13}$$

$$\rho_{gf} = r_{gf}\exp[i(\omega_S-\omega-\omega_{gf})t] + R_{gf}\exp[i(\omega_1+\omega_2+\omega_3-\omega-\omega_{gf})t],$$

$$\rho_{gk} = r_{gk}\exp[i(\omega_S-\omega_3-\omega-\omega_{gk})t] + R_{gk}\exp[i(\omega_1+\omega_2-\omega-\omega_{gk})t].$$

By substituting (13) into (12), one can see that the set of differential equations under consideration reduces to two independent sets of algebraic equations, where each refers to the processes determined by only one weak field:

$$iR_{gm}D_{gm} = -G_{gm} - R_{gn}G_{nm},$$

$$D_{gm} = \Gamma_{gm} + i(\omega_1-\omega_{gm}),$$

$$iR_{gn}D_{gn} = -\int R_{g\varepsilon}G_{\varepsilon n}d\varepsilon - R_{gm}G_{mn} - R_{gk}G_{kn},$$

$$D_{gn} = \Gamma_{gn} + i(\omega_1+\omega_2-\omega_{gn}),$$

$$iR_{g\varepsilon}D_{g\varepsilon} = -R_{gn}G_{n\varepsilon} - R_{gf}G_{f\varepsilon},$$

$$D_{g\varepsilon} = i(\omega_1+\omega_2+\omega_3-\omega_{g\varepsilon}), \tag{14}$$

$$iR_{gf}D_{gf} = -\int R_{g\varepsilon}G_{\varepsilon f}d\varepsilon - R_{gk}G_{kf},$$

$$D_{gf} = \Gamma_{gf} + i(\omega_1+\omega_2+\omega_3-\omega-\omega_{gf}),$$

$$iR_{gk}D_{gk} = -(R_{gn}G_{nk} - R_{gf}G_{fk}),$$

$$D_{gk} = \Gamma_{gk} + i(\omega_1+\omega_2-\omega-\omega_{gk}),$$

$$ir_{g\varepsilon}p_{g\varepsilon} = -G_{g\varepsilon} - r_{gn}G_{n\varepsilon} - r_{gf}G_{f\varepsilon},$$

$$p_{g\varepsilon} = i(\omega_S-\omega_{g\varepsilon}),$$

$$ir_{gn}p_{gn} = -\int r_{g\varepsilon}G_{\varepsilon n}d\varepsilon - r_{gm}G_{mn} - r_{gk}G_{kn},$$

$$p_{gn} = \Gamma_{gn} + i(\omega_S-\omega_3-\omega_{gn}), \tag{15}$$

$$ir_{gm}p_{gm} = -r_{gn}G_{nm},$$

$$p_{gm} = \Gamma_{gm} + i(\omega_S-\omega_3-\omega_2-\omega_{gm}),$$

$$ir_{gf}p_{gf} = -\int r_{g\varepsilon}G_{\varepsilon f}d\varepsilon - r_{gk}G_{kf},$$

$$p_{gf} = \Gamma_{gf} + i(\omega_S-\omega-\omega_{gf}),$$

$$ir_{gk}p_{gk} = -r_{gn}G_{nk} - r_{gf}G_{fk},$$

$$p_{gk} = \Gamma_{gk} + i(\omega_S-\omega_3-\omega-\omega_{gk}).$$

Here and elsewhere, the repeated index k indicates summation over all discrete off-resonant levels combined to form the level k.

Equations (14) describe the absorption of E_1 and generation at the frequency ω_S, and (15) presents the absorption of E_S and the parametric conversion of E_S back into E_1. One can solve (14) by substituting the equation for $R_{g\varepsilon}$ under the integrals. Then, in the calculation of the integrals, one can employ the ζ function,

$$[-i(\omega_S-\omega_{\varepsilon g})]^{-1} = \pi\delta(\omega_S-\omega_{\varepsilon g}) + i\mathrm{P}(\omega_S-\omega_{\varepsilon g})^{-1}, \tag{16}$$

where $\delta(\xi)$ is the delta function, and P is the principal value obtained by integration. This leads to the following equations:

$$R_{g\varepsilon} = i\left[G_{n\varepsilon} - (1-iq_{nf})\frac{\gamma_{nf}G_{f\varepsilon}}{\gamma_{ff}X_f}\beta_f\right]\frac{R_{gn}}{D_{g\varepsilon}},$$

$$R_{gm} = i\frac{G_{gm}+R_{gn}G_{nm}}{X_m\Gamma_{gm}}, \tag{17}$$

$$R_{gn} = -\frac{G_{gm}G_{mn}X_f}{\Gamma_{gm}\Gamma_{gn}X_m(1+g_{nn})(X_nX_f-K+A_mX_f)},$$

where

$$\beta_f = g_{ff}/(1+g_{ff}),\quad \beta_n = g_{nn}/(1+g_{nn}),$$

$$g_{ff} = \gamma_{ff}/\Gamma_{gf},\quad g_{nn} = \gamma_{nn}/\Gamma_{gn},$$

$$g_{mn} = |G_{mn}|^2/\Gamma_{gm}\Gamma_{gn},\quad q_{ij} = \delta_{ij}/\gamma_{ij}, \tag{18}$$

$$\gamma_{ij} = \pi\hbar G_{i\varepsilon}G_{\varepsilon j}\big|_{\varepsilon=\hbar\omega_S} + \mathrm{Re}(G_{ik}G_{kj}/p_{gk}),$$

$$\delta_{ij} = \mathrm{Im}\left[i\hbar P\int d\varepsilon\frac{G_{i\varepsilon}G_{\varepsilon j}}{(\hbar\omega_S-\varepsilon)} + G_{ik}G_{kj}/p_{gk}\right],$$

$$K = k_1\beta_f\beta_n(1-iq_{nf})(1-iq_{fn}),$$

$$A_m = g_{mn}/X_m(1+g_{nn}),$$

$$X_i = 1+ix_i,\ x_m = \Omega_1/\Gamma_{gm},$$

$$x_n = (\Omega_1 + \Omega_2 - \delta_{nn})/(\Gamma_{gn} + \gamma_{nn}) = (\omega_S - \omega_3 - \delta_{nn})/(\Gamma_{gn} + \gamma_{nn}),$$

$$x_f = (\Omega_1 + \Omega_2 - \Omega_L - \delta_{ff})/(\Gamma_{gf} + \gamma_{ff}) = (\omega_S - \omega - \omega_{gf} - \delta_{ff})/(\Gamma_{gf} + \gamma_{ff}),$$

$$\Omega_L = (\omega + \omega_{gf}) - (\omega_3 + \omega_{gn}),$$

$$\Omega_1 = \omega_1 - \omega_{gm}, \quad \Omega_2 = \omega_2 - \omega_{mn}. \tag{19}$$

Here Ω_L is the spacing between the quasilevels induced by the radiations E and E_3 in the continuum. The Fano parameters q_{ij} [19] are assumed real and indicate the ratio of the light-induced shifts and the broadening of the corresponding resonances by the control fields. In the adopted approximation, these parameters are independent of the field intensities and are governed solely by the properties of the investigated atom. The factor k_1 and other factors k_i used below are:

$$k_1 = \gamma_{nf}\gamma_{fn}/\gamma_{nn}\gamma_{ff},$$

$$k_2 = \gamma_{gf}\gamma_{fg}/\gamma_{gg}\gamma_{ff},$$

$$k_3 = \gamma_{gn}\gamma_{ng}/\gamma_{gg}\gamma_{nn},$$

$$k_4 = \gamma_{gf}\gamma_{fn}\gamma_{ng}/\gamma_{gg}\gamma_{ff}\gamma_{nn},$$

$$k_5 = \gamma_{gn}\gamma_{nf}\gamma_{fg}/\gamma_{gg}\gamma_{ff}\gamma_{nn},$$

$$k_6 = \gamma_{nf}\gamma_{fg}/\gamma_{ff}\gamma_{ng}. \tag{20}$$

They account for degenerate continuum states and are independent of the fields intensities. For nondegenerate continuum states they are equal to unity, while for the degenerate case these factors may become appreciably less than unity. These values are similar to the squared overlapping parameter

$$\rho^2 = |\langle \Psi_d | \Psi_a \rangle|^2$$

for the wave functions

$$\Psi_d = (\pi\hbar)^{1/2}\frac{\sum_j G^j_{d\epsilon_0}\psi^j_{\epsilon_0}}{(\sum_j \gamma^j_{dd})^{1/2}}, \quad \Psi_a = (\pi\hbar)^{1/2}\frac{\sum_j G^j_{a\epsilon_0}\psi^j_{\epsilon_0}}{(\sum_j \gamma^j_{aa})^{1/2}}$$

of the continuum states ϵ_d and ϵ_a, excited from the levels d and a.

Following the same procedure as above and bearing in mind the condition $\omega_S = \omega_1 + \omega_2 + \omega_3$, one finds from the set of equations (15) that

$$r_{g\varepsilon} = i\{G_{g\varepsilon} - G_{f\varepsilon}(\gamma_{gf}/\gamma_{ff})\beta_f(1 - iq_{gf})/X_f + r_{gn}[G_{n\varepsilon} - G_{f\varepsilon}(\gamma_{nf}/\gamma_{ff})\beta_f(1 - iq_{nf})/X_f]\}/p_{g\varepsilon},$$

$$r_{gm} = i\frac{r_{gn}G_{nm}}{X_m\Gamma_{gm}}, \tag{21}$$

$$r_{gn} = \frac{(1 - iq_{fn})(1 - iq_{gf})\gamma_{gf}\gamma_{fn}/(\Gamma_{gf} + \gamma_{ff}) - (1 - iq_{gn})X_f\gamma_{gn}}{(1 + g_{nn})\Gamma_{gn}(X_fX_n - K + A_mX_f)}.$$

With the aid of the equations for R_{gm} calculated from (17), and for $r_{g\varepsilon}$ calculated from (21), and with Eqs. (10) and (11), after integration over the continuum states, one can obtain the following expressions for the absorption and refractive indices at the frequencies ω_1 and ω_S, respectively:

$$\frac{\alpha(\omega_1)}{\alpha_{10}} = \mathrm{Re}F_1, \quad \frac{n(\omega_1) - 1}{\alpha_{10}\lambda_1/2} = \mathrm{Im}F_1, \quad F_1 = \frac{1}{X_m}\left[1 - \frac{A_mX_f}{X_nX_f + A_mX_f - K}\right], \tag{22}$$

$$\frac{\alpha(\omega_S)}{\alpha_{S0}} = \mathrm{Re}F_S, \quad \frac{n(\omega_S) - n_{S0}}{\alpha_{S0}\lambda_S/2} = \mathrm{Im}F_S, \tag{23}$$

$$F_S = \left[1 - \frac{X_fX_n(A_n + A_f) - U + A_mA_fX_f}{X_fX_n - K + A_mX_f}\right] = \left[1 - A_f - A_n - \frac{K(A_n + A_f) - U - A_mA_nX_f}{X_fX_n - K + A_mX_f}\right] = \left[1 - A_f - \tilde{A}_n - \frac{K(\tilde{A}_n + A_f) - U}{X_f\tilde{X}_n - K}\right].$$

Here α_{10} is the resonant value of the absorption index at the wavelength λ_1 with all strong fields turned off; α_{S0} and n_{S0} are similar quantities for the absorption and refractive indices at the wavelength λ_S; and

$$A_f = \beta_f k_2(1 - iq_{gf})(1 - iq_{fg})/X_f,$$

$$A_n = \beta_n k_3(1 - iq_{gn})(1 - iq_{ng})/X_n,$$

$$U = \beta_f\beta_n[k_4(1 - iq_{gf})(1 - iq_{fn})(1 - iq_{ng}) + k_5(1 - iq_{gn})(1 - iq_{nf})(1 - iq_{fg})], \tag{24}$$

$$\tilde{A}_n = \beta_n k_3(1 - iq_{gn})(1 - iq_{ng})/\tilde{X}_n,$$

$$\tilde{X}_n = X_n + A_m.$$

The functions $\tilde{A}_n$ and $\tilde{X}_n$ account for the perturbation of a two-photon resonance with the level n by the strong fields. The expressions for the refractive index are obtained under the assumption that this index is close to unity in the absence of the fields.

The equation for the FWM nonlinear susceptibility at $\omega_S = \omega_1 + \omega_2 + \omega_3$ calculated with the aid of Eqs. (10), (11), and (17) after integration over the continuum states, $\int d\varepsilon R_{g\varepsilon}d_{\varepsilon g}$, is given by

$$\frac{\chi^{(3)}(\omega_S)}{\chi^{(3)}_{S0}} = \frac{X_f - k_6\beta_f(1 - iq_{fg})(1 - iq_{nf})/(1 - iq_{ng})}{X_m(1 + g_{nn})(X_nX_f - K + A_mX_f)}, \tag{25}$$

where $\chi^{(3)}_{S0}$ is the fully resonant nonlinear susceptibility at $E_{2,3}$, $E \to 0$.

IV. LASER-INDUCED STRUCTURES IN DISCRETE AND CONTINUOUS SPECTRA OF ABSORPTION AND REFRACTION

In this section, we investigate coherent control of absorption and refractive indices in the vicinity of discrete and within continuous quantum transitions with the aid of Eqs. (22) and (23). As seen from Eq. (22), the strong field E_2, in cooperation with the other two, substantially modifies the absorption and dispersive indices at ω_1. An important difference is seen when compared with similar effects at solely discrete transitions [2,3,5,6]. The results given below demonstrate considerable perturbations of discrete spectra by the radiations coupled to the continuum. The first term in (22) represents the field-unperturbed absorption index for the *gn* transition (at $A_m=0$), and the second term refers to the cumulative effects of the strong fields. The coefficient A_m determines the splitting of a resonance into two components by the strong field E_2 [2,3,5,6], which is modified by the strong field E_3. The function K describes further modification of the absorption index by the strong field E. It is proportional to the product of the intensities of the fields E and E_3, and the effect disappears when any of these fields is turned off. Since the field E_2 is in resonance with a discrete transition and the fields E_3 and E are coupled to the continuum, the spectral properties of the corresponding contributions are different. If $E=0$ (i.e., $g_f=\gamma_f=\beta_f=K=0$), the equation for the absorption index (22) converges to the standard one commonly used in three-level nonlinear spectroscopy [2,3,5,6]:

$$\frac{\alpha(\omega_1)}{\alpha_{01}} = \mathrm{Re}\left[X_n \Big/ \left(X_n X_m + \frac{g_{mn}}{1+g_{nn}} \right) \right]. \qquad (26)$$

The denominator in (26) has two roots with respect to $\Omega_1 = \omega_1 - \omega_{mn}$, which indicates a splitting of the resonance into two maxima. The positions of these maxima and their relative amplitudes may vary depending on the parameters of the fields and transitions. Resonance splitting is stipulated by the appearance of coherence at the transition *ng*, which is associated with the appearance of additional quantum transitions *ng* in which photons of frequency $\hbar\omega_1$ may participate. The corresponding laser-induced resonances (quasilevels) are shown by the dashed lines in Fig. 1. The phase and relaxation properties of the respective term for the polarization at frequency ω_1 are reflected by the dispersion function X_n. The additional strong fields E_3 and E cause further modification of the laser-induced quasilevels. Corresponding changes occur in the absorption (Fig. 2) and refractive indices [Fig. 2(b,dash)], which constitutes the base for their quantum control.

This figure displays the dependence of the absorption index at ω_1 on the scaled detunings from the bare-state one-photon resonance, $\omega_1-\omega_{gm}$. Here, Γ_{ij} is the homogeneous halfwidth of the ij transition, Ω_2 is the frequency deviation of the second field from the transition *mn*, g_{mn} is the squared scaled Rabi frequency for this field, g_{nn} and g_{ff} are the equivalent values for coupling of the corresponding level with the continuum, and q_{ij} are Fano parameters. All these denotations are given by Eqs. (18) and (19). The frequency detunings Ω_L and Ω are depicted in Fig. 1. We have selected

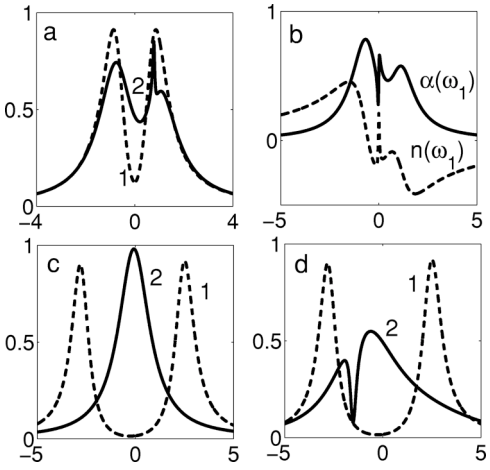

FIG. 2. Absorption index at ω_1 reduced by its resonant value in the absence of all strong fields, $\alpha(\omega_1)/\alpha_{10}$, vs scaled one-photon detuning $\Omega_1/\Gamma_{gm}=(\Omega_1=\omega_1-\omega_{gm})/\Gamma_{gm}$. Here, $q_{ff}=0.9$, $q_{nn}=0.5$, $\Gamma_{gm}/\Gamma_{gf}=100$, and $\Gamma_{gm}/\Gamma_{gn}=10$. (a,b): $\Omega_2=0$, $q_{fn}=1.5$, $g_{mn}=7$, $g_{ff}=2$. (a): $g_{nn}=0$ **(1)**, $g_{nn}=5$, $\Omega_L/\Gamma_{gm}=0.8$ **(2)**. (b): $g_{nn}=5$, $\Omega_L=0$. (c,d): $\Omega_2/\Gamma_{mn}=0.3$, $g_{mn}=70$, $g_{ff}=10$, $\Omega_L/\Gamma_{gm}=-1.1$, $g_{nn}=0$ **(1)**, $g_{nn}=50$ **(2)**. (c): $q_{fn}=15$. (d): $q_{fn}=1.5$.

numerical parameters from among those relevant to different experiments in order to illustrate the breadth of possible coherent control.

Figures 2(a) and 2(b) correspond to the dressing field E_2 being in exact resonance ($\Omega_2=0$). Plot 1 in Fig. 2(a) corresponds to $E_3=0$. The splitting of the resonance and the consequent decrease in the center of the bare-state resonance is produced with the strong field coupled to the transition *mn*. An additional dressing field at the frequency ω_3 may bring a dramatic change in the absorption line shape [plot 2, Fig. 2(a)]. Plots 1 and 2 in Fig. 2(a) present an example of possible modification of the absorption profile in the vicinity of a discrete transition by the fields coupling bound and free states. Figure 2(b) illustrates a significant change of the same line shape at the overlap of two LICS induced by the fields E_3 and E [compare plot 2 in Fig. 2(a) and plot $\alpha(\omega_1)$ in Fig. 2(b)]. This allows one to manipulate the transparency and refractive index for the resonant fundamental radiation E_1 through variation of the magnitude $\Omega_L=\omega-\omega_3-\omega_{nf}$. The dashed plot in Fig. 2(b) shows the line shape of the dispersive part of the refractive index at frequency ω_1 for the same parameters. The plot indicates the feasibility of the creation of extremely steep dispersion with the aid of the dressing field, coupled to both discrete and continuum states. Figures 2(c) and 2(d) show the interference structures induced by only the field E_2 (plot 1) and jointly by the two dressing fields E_3 and E (plot 2). Figure 2(c) displays possible control of the transparency window by the field E_3, including complete eradication of the effect by the field E_2 (plot 2). Figures 2(c) and 2(d) show that the interference structures induced jointly by the two dressing fields E_3 and E may strongly depend on the Fano parameter q_{fn} [compare plots 2(c) and 2(d)].

Overall, Fig. 2 shows the feasibility of *manipulating absorption and dispersive indices in the vicinity of discrete transitions by the control fields that couple discrete and con-*

tinuous states. It demonstrates that one can create transparency and steep dispersion in certain frequency intervals of the discrete transitions or, on the contrary, eliminate effects of the dressing fields with the aid of destructive interference by varying the intensities and detunings of the driving fields with account for the specific Fano parameters. These parameters present the relative contribution of the resonant continuum states, within the bandwidth on the order of the characteristic width of the power-broadened discrete resonance, and that of others integrated over all off-resonant continuous and discrete states. Such a ratio determines the phase shift of the intra-atomic oscillations brought about by the transitions to the continuum states.

The spectral characteristics of absorption at the frequency ω_S are determined by the interference of three quantum pathways: direct to the continuum, to level f, and to the superposition of levels n and m. The line shapes of the absorption and dispersive indices are presented by Eq. (23), whose structure is similar to (22). The first term presents the unperturbed absorption index, while the rest describe contributions of the additional quantum pathways induced by the dressing fields. The function A_f presents an autoionizinglike resonance induced by E, and the function $\tilde{A}_n$ describes the resonance induced by E_3 and modified by E_2. The factors K and U describe the interference of the above outlined processes, i.e., contributions of quantum pathways via various intermediate states, induced jointly by E_3 and E. Their appearances are determined by the Fano parameters. In the limiting case of $E_3=0$ (i.e., at $\tilde{A}_n=0, K=0, U=0$) and $k_3=1$, Eq. (23) reduces and converges to the corresponding equation from [6,17,18,21,23]

$$\frac{\alpha(\omega_S)}{\alpha_{S0}} = \mathrm{Re}\{1 - A_f\} = 1 - \beta_f + \beta_f \frac{(q_{gf} + x_f)^2}{1 + x_f^2}, \qquad (27)$$

where $x_f=(\omega_S-\omega-\omega_{gf}-\delta_{ff})/(\Gamma_{gf}+\gamma_{ff})$, and $\beta_f \to 1$ at $\gamma_{ff} \gg \Gamma_{gf}$. This equation is similar to that for a real autoionizing resonance [19]. It describes asymmetrical power-broadened (γ_{ff}) and power-shifted (δ_{ff}) resonance, whose asymmetry is determined by the Fano parameter q_{gf}. When $\beta_f \to 1$, the absorption profile is depicted only by the last term. In this case, *the absorption vanishes at* $x_f=-q_{gf}$ *and reaches its maximum value,* $\alpha_{S0}(1+q_{gf}^2)$, *at* $x_f=1/q_{gf}$. When the contribution of the resonant continuum states is relatively small ($q_{gf} \gg 1$), the absorption is predominantly determined by the two photon transition $g \to f$. Then the effect of interference of one- and two-photon transitions becomes small. Consequently the resonance profile becomes a symmetrical Lorentzian, and the transparency window vanishes. Otherwise, the asymmetry grows with $q_{gf} \to 0$. The location of the resonance is controlled by the frequency ω of the field E, and its strengths by β_f, i.e., by the strength of this field.

Strong fields E_3 and E_2 bring about further qualitative changes in the spectra. The additional independent structure, described in these expressions by the function $\tilde{A}_n$, is supplemented by the interference term, which depends on the factors K and U. This term disappears when either of the fields

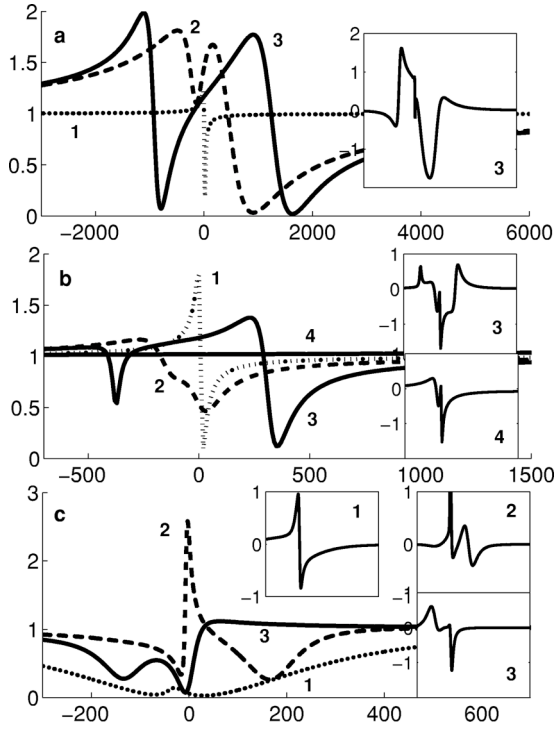

FIG. 3. Absorption index at ω_S reduced by its value in the absence of all strong fields, $\alpha(\omega_S)/\alpha_{S0}$, vs detunings $\Omega/\Gamma_{fg}=(\omega_S-\omega-\omega_{fg})/\Gamma_{fg}$ (a–c). The insets are the interference contributions to the corresponding curves vs detuning, the detuning interval is the same as for the main curves. Here, $\Gamma_{gm}/\Gamma_{gf}=100$, $\Gamma_{gm}/\Gamma_{gn}=10$. (a,b): $q_{ff}=0.9$, $q_{nn}=0.9$, $\Omega_L/\Gamma_{gf}=-110$, $\Omega_2/\Gamma_{gf}=30$. (a): $q_{gf}=-0.5$, $q_{gn}=-0.95$, $q_{fn}=15$. **(1)** $E_2=E_3=0$, $\gamma_{ff}/\Gamma_{gf}=10$. **(2–3)** $g_{mn}=70$, $\gamma_{nn}/\Gamma_{gn}=50$. **(2)** $\gamma_{ff}=0$. **(3)** $\gamma_{ff}=10$. (b): $q_{gf}=-0.95$, $q_{gn}=-0.5$, $q_{fn}=15$ **(2,3)**, $q_{fn}=150$ **(4)**. **(1)** $E_2=E_3=0$, $\gamma_{ff}/\Gamma_{gf}=10$. **(2–4)** $g_{mn}=7$, $\gamma_{nn}/\Gamma_{gn}=5$. **(2)** $\gamma_{ff}=0$. **(3,4)** $\gamma_{ff}/\Gamma_{gf}=10$. (c): $q_{gf}=0.95$, $q_{gn}=0.01$, $q_{ff}=0.01$, $q_{nn}=-5$, $q_{fn}=1.5$, $\Omega_2/\Gamma_{gf}=0$, $\gamma_{ff}/\Gamma_{gf}=10$, $g_{mn}=7$. **(1)** $\gamma_{nn}/\Gamma_{gn}=30$, $\Omega_L/\Gamma_{gl}=-1530$. **(2,3)** $\gamma_{nn}/\Gamma_{gn}=5$. **(2)** $\Omega_L/\Gamma_{gf}=-110$. **(3)** $\Omega_L/\Gamma_{gf}=-405$.

E_3 or E is turned off or when the spacing Ω_L between the LICS is increased.

The plots in Fig. 3 show the dependence of the absorption index at frequency ω_S on scaled detuning $\omega_S-(\omega+\omega_{fg})$. The magnitudes of the parameters used for the simulation, as given in the figure captions, are selected to illustrate the feasible manipulation of quantum interference and its dependence on the atomic parameters. In Figs. 3(a) and 3(b), plots 1 correspond to fields E_2 and E_3 being turned off and display characteristic asymmetric laser-induced Fano resonances [Eq. (27)], plots 2 display the cases for $E=0$, and plots 3 depict the case when all three fields are turned on. The plots show strong dependence of the absorption index on the Fano parameters, q_{gf} and q_{gn} in the cases discussed, and feasibilities for manipulating quantum interference by LICS with supplementary dressing fields that couple the adjacent transitions. Interference contributions, which disappear in the absence of either E or E_3, are shown in the insets to the figure. Due to the interference nature, a frequency integral in each of them equals to zero. Plot 4 in Fig. 3(b) demonstrates the feasibility of mutual suppression of LICS through their destructive interference, so that the absorption spectrum be-

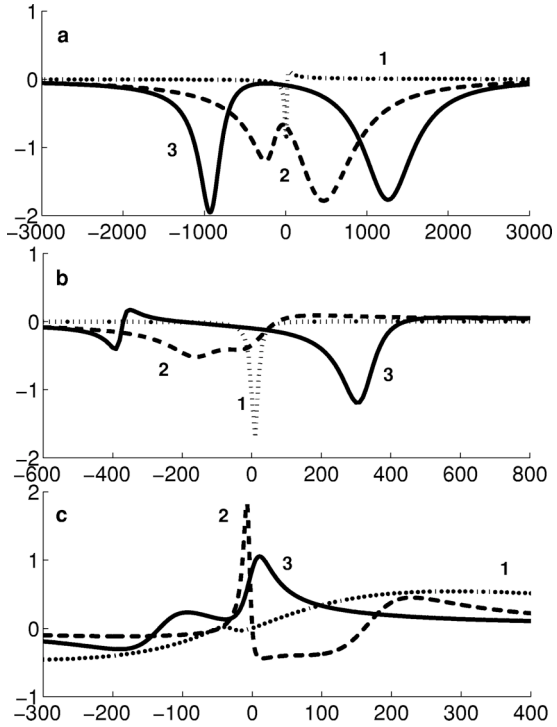

FIG. 4. Scaled laser-induced change of the dispersive part of the refractive index at ω_S in the vicinity of LICS vs $\Omega/\Gamma_{fg}=(\omega_S-\omega-\omega_{fg})/\Gamma_{fg}$. All parameters are the same as for the corresponding plots (a–c) in Fig. 3.

comes the same as in the case of all strong fields being turned off. Variation of the parameter q_{fn} leads to an appreciable change in the shape of laser-induced structures (compare plots 3 and 4).

Figure 3(c) shows the dependence of the absorption spectrum on the strength of the driving field E_3 as well as on the spacing between two quasilevels induced in the continuum by E and E_3. In regard to the detuning $\Omega_L=\omega-\omega_3-\omega_{fn}$, plot 1 corresponds to large detuning ($\Omega_L/\Gamma_{gf}=-1530$), plot 2 to small detuning ($\Omega_L/\Gamma_{gf}=-110$), and plot 3 to medium detuning ($\Omega_L/\Gamma_{gf}=-405$). The appearance of LICS is most pronounced in the last case.

Figure 3 demonstrates the possible manipulation of the absorption index for a probe radiation by LICS that includes formation of the transparency windows. Opportunities are brought about by the interference of two LICS, i.e., quantum pathways via continuum states induced jointly by the fields at ω_3 and ω and modified by the strong field at ω_2. The interference term displayed in the insets shows that the magnitude of this term is comparable with others and can be both constructive and distractive, depending on detunings of $\omega-\omega_3$ from ω_{nf}, as well as on the Fano parameters, and on the intensities of the coupled fields.

Figure 4 displays the feasibilities of manipulating by the magnitude and profile of LICS in the refractive index. Such artificial dispersive structures are superimposed over a flat background and can be manipulated by a change of intensities and of frequencies of the dressing fields with the account for a strong dependence of the interference processes on the Fano parameters. The figure demonstrates the *feasibility of creation of very steep variable positive and negative dispersion for the short wavelength radiation* with the aid of coherence and interference processes associated with the continuum states.

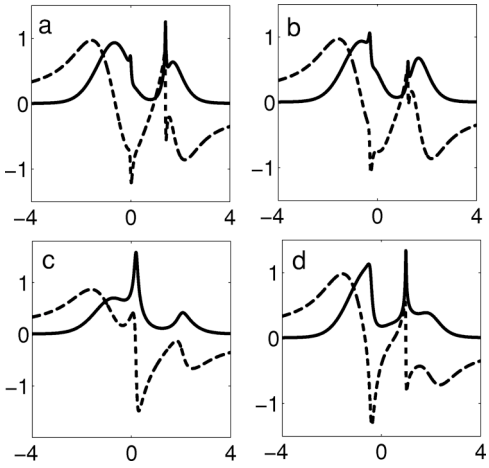

FIG. 5. Velocity averaged absorption index, $\langle\alpha(\omega_1)\rangle/\langle\alpha_{10}\rangle$, (solid) and dispersion part of the refractive index (dash) at ω_1 reduced by their maximum values in the absence of all strong fields in a Doppler-broadened medium vs $\Omega_1/\Delta\omega_{1D}$. Here, the Doppler HWHM $\Delta\omega_{1D}=16.65\,\Gamma_{gm}$, the wave vector orientations are $\mathbf{k}\uparrow\uparrow\mathbf{k}_1$, $\mathbf{k}_2\uparrow\uparrow\mathbf{k}_3\uparrow\downarrow\mathbf{k}_1$, and $k_2/k_1=0.9$, $k_3/k_1=0.5$, $k/k_1=0.6$ ($\mathbf{k}_i$ is wave vector corresponding to the frequency ω_i), $\Gamma_{gm}/\Gamma_{gf}=100$, $\Gamma_{gm}/\Gamma_{gn}=10$; $|G_{mn}|^2/(\Delta\omega_{1D})^2=1$, $q_{nn}=0.5$, $q_{ff}=0.9$, $\Omega_2/\Delta\omega_{1D}=-0.9$. (a,b): $\gamma_{nn}/\Delta\omega_{1D}=0.1$, $\gamma_{ff}/\Delta\omega_{1D}=0.2$, $q_{fn}=0.5$. (a): $\Omega_L=0$. (b–d): $\Omega_L/\Delta\omega_{1D}=-0.8$. (c): $\gamma_{nn}/\Delta\omega_{1D}=0.8$, $\gamma_{ff}/\Delta\omega_{1D}=0.3$, $q_{fn}=-1.5$. (d): $\gamma_{nn}/\Delta\omega_{1D}=0.2$, $\gamma_{ff}/\Delta\omega_{1D}=0.8$, $q_{fn}=1.5$.

The above demonstrated features of quantum interference and continuum coherence can be considered as candidates for application to the persistent problems in the design of such optical elements in the vacuum-ultraviolet wavelength range as tunable narrowband filters, polarization rotators, and dispersive elements.

V. ABSORPTION AND REFRACTIVE SPECTRA AT DOPPLER-BROADENED TRANSITIONS

Homogeneously broadened discrete transitions with near Lorentzian profile of resonance can be observed in atomic jets or by immersing resonant atoms into a high-pressure buffer gas. Basically, the Maxwell distribution of atoms over velocities in warm gases and metal vapors leads to a corresponding exponential distribution of Doppler shifts of narrow Lorentzian resonances. This may substantially change the features described above. In this section we shall illustrate such changes with the example of Doppler broadened media. Among the important features is the dependence of the spectra on the ratio of the frequencies and on the relative orientation of wave vectors of the coupled waves.

Figure 5 shows the feasibility of the modification of the Doppler-broadened absorption resonance at ω_1 and the creation of a dramatically changed profile with new maxima. Thus, instead of a Gaussian contour centered at $\Omega_1=0$ with half width at half maximum (HWHM) about 1, the plot in

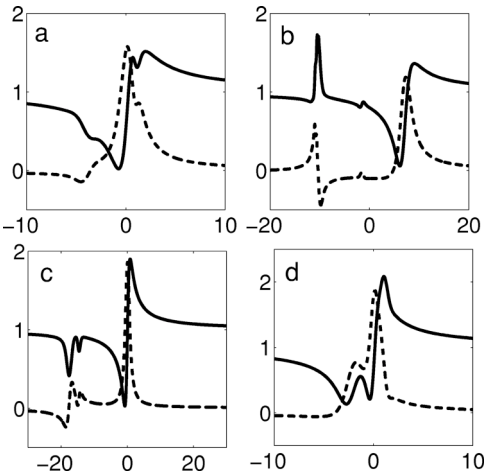

FIG. 6. Velocity-averaged absorption index, $\langle\alpha(\omega_S)\rangle/\langle\alpha_{S0}\rangle$, (solid) and dispersion part of the refractive index (dash) at ω_S reduced by their values in the absence of all strong fields in a Doppler-broadened medium vs detuning $\Omega/\Delta\omega_{SD}=(\omega_S-\omega-\omega_{fg})/\Delta\omega_{SD}$. Here, the Doppler HWHM $\Delta\omega_{SD}=5\times10^3\,\Gamma_{gf}$; the wave vector orientations are the same $\mathbf{k}\uparrow\uparrow\mathbf{k}_3\uparrow\uparrow\mathbf{k}_2\uparrow\uparrow\mathbf{k}_S$, and $k/k_S=0.8$, $k_3/k_S=0.3$, $k_2/k_S=0.37$, $\Gamma_{gm}/\Gamma_{gf}=100$, $\Gamma_{gm}/\Gamma_{gn}=10$; $|G_{mn}|^2/(\Delta\omega_{SD})^2=1$, $\gamma_{nn}/\Delta\omega_{SD}=0.4$, $\gamma_{ff}/\Delta\omega_{SD}=0.8$, $q_{gf}=0.95$, $q_{gn}=0.01$, $q_{ff}=0.01$, $q_{nn}=-5$. (a): $q_{fn}=1.5$, $\Omega_L/\Delta\omega_{SD}=1.5$, $\Omega_2/\Delta\omega_{SD}=2.2$. (b–d): $\Omega_2=0$. (b): $q_{fn}=15$, $\Omega_L/\Delta\omega_{SD}=1.5$. (c): $q_{fn}=-1.5$, $\Omega_L/\Delta\omega_{SD}=15$. (d): $q_{fn}=-1.5$, $\Omega_L/\Delta\omega_{SD}=-0.5$.

Fig. 5(a) displays the profile of almost the same Gaussian shape shifted by about 0.5 HWHM, an *enhanced narrow sub-Doppler resonance* shifted to the opposite side at about two HWHM, and the transparency window between them. Due to the pure interference nature of the effect, the integral value of the index taken over Ω_1 must not change. Because of the difference between ω_1 and ω_2, the compensation of their Doppler shifts at two-photon transition *gn* in counterpropagating weak waves is not possible. However, for an appropriate choice of the coupling parameters, such compensation of the Doppler shift with velocity-dependent power shifts caused by the dressing fields becomes possible. For details of the physics in more simple cases, see [2,28] and references therein. Indeed, this effect exhibits itself as the appearance of an enhanced sub-Doppler peak. Such a peak can be created through the overlap of two LICS [Fig. 5(a)] or through the adjustment of another appropriate combination of atomic and field parameters [Fig. 5(d)]. Other possible modifications of the absorption profile are presented in Fig. 5(b) and 5(c). It is seen that the properties of the continuum presented by the given values of the Fano parameters play an important role. Corresponding changes occur in refractive index and in nonlinear susceptibilities.

Figures 6(a)–6(d) shows similar opportunities for manipulating absorption and refractive indices in Doppler-broadened gases for otherwise unstructured continuous spectra. These figures demonstrate an almost vanished absorption created through destructive interference. Either single [(a–c)] or multiple [(a–d)] transparency windows can be created.

Figures 5 and 6 demonstrate that the interference of contributions from the atoms at different velocities brings an important distinction in the appearance of quantum interference processes at coupled discrete and continuous transitions. The figures show that such interference may also be constructive or destructive, depending on the sign of the detuning $\omega-\omega_3-\omega_{nf}$, on the Fano parameters, on the detunings from the two-photon resonance *gn*, on the ratio of the frequencies, and on the orientations of the wave vectors of the coupled electromagnetic waves. The plots show that the proper adjustment of the orientation of the wave vectors, along with the intensities and detunings of the coupled waves provides the additional means of manipulating the line shape of Doppler-broadened transitions. Thus *sub-Doppler frequency-tunable transparency windows, enhanced absorption, and steep negative or positive dispersion structures can be created* through compensation for Doppler shifts by velocity-dependent power shifts of the atomic resonances.

VI. RESONANCE SUM-FREQUENCY GENERATION IN STRONGLY ABSORBING MEDIA ENHANCED BY QUANTUM INTERFERENCE

Nonlinear interference structures, similar to those discussed above, can be created in the real and imaginary parts of nonlinear FWM susceptibility as well. As shown for the first time in [18], the NIE may influence differently the linear and nonlinear susceptibilities, so that under certain conditions a *reduction in the absorption of the generated radiation may lead to no decrease in FWM polarization*. For example, when E_2 and E_3 are nonperturbatively small and the continuum is nondegenerate, the equation (25) reduces to

$$\frac{\chi^{(3)}(\omega_S)}{\chi^{(3)}_{S0}}=\frac{1}{X_mX_n}\left[1-\beta_f\frac{(1-iq_{fg})(1-iq_{nf})}{(1-iq_{ng})(1+ix_f)}\right], \qquad (28)$$

where x_f is scaled detuning Ω given by Eq. (19). As one can see from Eq. (17) for $R_{g\varepsilon}$, the first term presents FWM process $\omega_S=\omega_1+\omega_2+\omega_3$, whereas the second interfering component originates from the higher-order process $\omega_S=\omega_1+\omega_2+\omega_3-\omega+\omega$. The second term depicts an asymmetric resonance as the function of ω_3 or ω. Its maximum is achievable at $\beta_f\to1$. Depending on the other parameters, this term may either fully compensate the first one and thus terminate the FWM response, or alternatively, enhance it. As it was shown above [see the discussion on Eq. (27)], *the absorption of generated radiation vanishes at* $x_f=-q_{fg}$ *whereas*, according to Eq. (28), *the FWM polarization may even significantly increase*, if $q_{nf}\gg q_{ng}$ [18].

In weak fields, the nonlinear susceptibility increases strongly upon approaching discrete resonances. However, this is accompanied by the significant growth in the absorption of the radiations. Hence, the trade-off modification of the nonlinear FWM polarization on one hand, and the absorption and refractive indices on the other hand, become a most important problem in maximizing the generation output. Unlike the spectra discussed above, ω_1 and ω_S are locked and cannot be varied independently in the course of FWM. The trade off also depends on whether the local FWM conversion rate exceeds the absorption rate or vice versa, and if so, which absorption dominates in a given experimental scheme. Therefore, the creation of the nonlinear resonances

in nonlinear polarization must be performed in the context of optimization of the parameters of the overall local conversion rate b [Eq. (8)]. Ultimately, the trade-off options depend on which of the oscillator strength of the transitions, composing the coupling scheme, dominates. In this section we shall investigate such options based on LICS produced with several strong fields. The aim is to explore the opportunities for increasing the conversion efficiency with the aid of the control field. Such a field does not contribute to FWM directly, but allows one to adjust the interfering quantum channels contributing to the overall process in order to maximize the generation output. We shall investigate the corresponding evolution of the generated radiation along the medium. For the sake of simplicity, we assume the medium to be homogeneously broadened, the continuum to be single (all parameters $k_i=1$), and phase mismatch to be ensured by the buffer gas.

A numerical analysis of the interplay of the outlined processes is convenient to perform with the aid of expression (7) rewritten in the form:

$$\eta_q(z) = \frac{4\overline{\eta}_{q0}}{|\overline{b}|}\exp[-(\overline{\alpha}_1 + C\overline{\alpha}_S)z\alpha_{10}/2] \times \{\sinh^2[\sqrt{(|\overline{b}| - \overline{b})C/2}z\alpha_{10}/2] + \sin^2[\sqrt{(|\overline{b}| + \overline{b})C/2}z\alpha_{10}/2]\}, \tag{29}$$

where

$$\overline{\eta}_{q0} = \frac{\tilde{\eta}_{q0}}{\alpha_{10}\alpha_{S0}}, \quad \overline{\alpha}_1 = \frac{\alpha_1}{\alpha_{10}}, \quad \overline{\alpha}_S = \frac{\alpha_S}{\alpha_{S0}}, \quad C = \frac{\alpha_{S0}}{\alpha_{10}},$$
$$\overline{b} = b/\alpha_{10}\alpha_{S0} = 4\overline{\eta}_{q^0} - (\overline{\alpha}_1 - C\overline{\alpha}_S)^2/4C. \tag{30}$$

Herewith, we have introduced the optical density $z\alpha_{10}$ of the resonant medium for E_1, the reduced absorption indices discussed above, and the ratio C of the nonperturbed absorption indices at ω_S and its resonant value at ω_1. Since C is proportional to the ratio of the oscillator strengths of the corresponding transitions, it specifies the atomic medium. The term $\overline{\eta}_{q0}$ is proportional to the squared modulus of the FWM nonlinear susceptibility and gives the quantum conversion efficiency over a characteristic absorption length $1/\sqrt{\alpha_{10}\alpha_{S0}}$ considered within the approximation of ignoring absorption of the given fields. It can be further presented in a more explicit form,

$$\overline{\eta}_{q0} = \eta^0_{q0}|\overline{\chi}^{(3)}|^2 g_{mn}g_{nn}, \tag{31}$$

where

$$\eta^0_{q0} = \frac{k_1'k_S'|2\pi\chi_0|^2}{\alpha_{10}\alpha_{S0}}\frac{16\hbar^3\Gamma_{gm}\Gamma^2_{gn}}{\pi|d_{mn}d_{n\varepsilon}|^2} \tag{32}$$

is the efficiency for the resonant unperturbed nonlinearity over a distance $1/\sqrt{\alpha_{10}\alpha_{S0}}$ in the fields corresponding to $g_{mn}=g_{nn}=1$. The reduced nonlinear susceptibility, $\overline{\chi}^{(3)} = \chi^{(3)}_S/\chi_{S0}$, is given by Eq. (25), where χ_{S0} is the fully (one- and two-photon) resonant value of the susceptibility for negligibly weak fields. We shall henceforth use the following approximate expressions:

$$\alpha_{10} = 4\pi\omega_1 N|d_{gm}|^2/c\hbar\Gamma_{gm},$$
$$\alpha_{S0} = 4\pi^2(\omega_S/c)N|d_{g\varepsilon}|^2(\varepsilon = \hbar\omega_S), \tag{33}$$
$$|\chi_0|^2 = (\pi/2\hbar^2)^2 N(1+q^2_{gn})|d_{gm}d_{mn}d_{n\varepsilon}d_{\varepsilon g}|^2(\Gamma_{gm}\Gamma_{gn})^{-2}.$$

Then Eq. (32) reduces to

$$\eta^0_{q0} = 1 + q^2_{gn}. \tag{34}$$

Therefore, in such approximation, the factor η^0_{q0} is determined only by the Fano parameter q_{gn}.

As discussed above, the appearance of laser-induced resonances for radiation E_1 can be interpreted as a splitting of the level m into quasilevels by the strong field E_2 and by their further modification by the fields E_3 and E. The laser-induced resonances for the generated radiation are determined by the creation of two quasilevels embedded in the continuum that appear near the frequencies $\omega_{ng}+\omega_3$ and $\omega_{fg}+\omega$. These quasilevels are separated by an energy $\hbar\Omega_L$. The detuning of the generated frequency from the first resonance is $\Omega_S=\Omega_1+\Omega_2$, whereas that from the second resonance is $\Omega=\Omega_S-\Omega_L$. The result is obviously different depending on whether these detunings are varied at the expense of deviations from one- and two-photon resonances, Ω_1 and Ω_2, or solely by changing the magnitude $\Omega_L=\omega-\omega_3-\omega_{fn}$. The relative role of these channels also depends on the intensities of the radiations, on their detunings from the resonances, and on the relative magnitudes of the oscillator strengths for the transitions gm and $g\varepsilon$. We shall illustrate the outlined dependencies through investigation of several numerical models of the medium.

Figure 7 depicts the case where the absorption of the generated radiation is considerably less than the *resonant* absorption at the transition gm ($C=10^{-5}$). The frequencies ω_1 and ω_2 are considerably detuned from their one-photon resonances, but the sum of the frequencies is close to a perturbed two-photon resonance. It is seen from Fig. 7(a) that, for the selected coupling and Fano parameters, the variation of Ω_L by change of the frequencies ω or ω_3 may provide approximately a threefold reduction of the absorption coefficient α_1, whereas α_S increases approximately by a factor of 3.8 in some detuning interval, and considerably decreases in other intervals. As such, the squared modulus of the nonlinear polarization, which is proportional to $\overline{\eta}_{q0}$, increases by a factor of 1.9. These are changes that, when estimated, compared to the values of the corresponding parameters in the far wings of the plots, where the effects of the control field E vanish. The absorption coefficient for a transition to the continuum, however, remains much less than α_1, so that $\alpha_S/\alpha_1 = C\overline{\alpha}_S/\overline{\alpha}_1 \approx 10^{-2}$ over the whole considered interval of Ω_L. In some range of Ω_L, the sign of $\overline{b}$ becomes positive, which indicates that the nonlinear-optical conversion rate begins to exceed the rate of absorption of the radiation. Indeed, within this interval of Ω_L, a sharp maximum of conversion develops [Fig. 7(c)]. The maximum $\eta_{q\ \max}=0.29$ is reached for $z\alpha_{10}=4000$. Figure 7(b) shows that outside this optimum match,

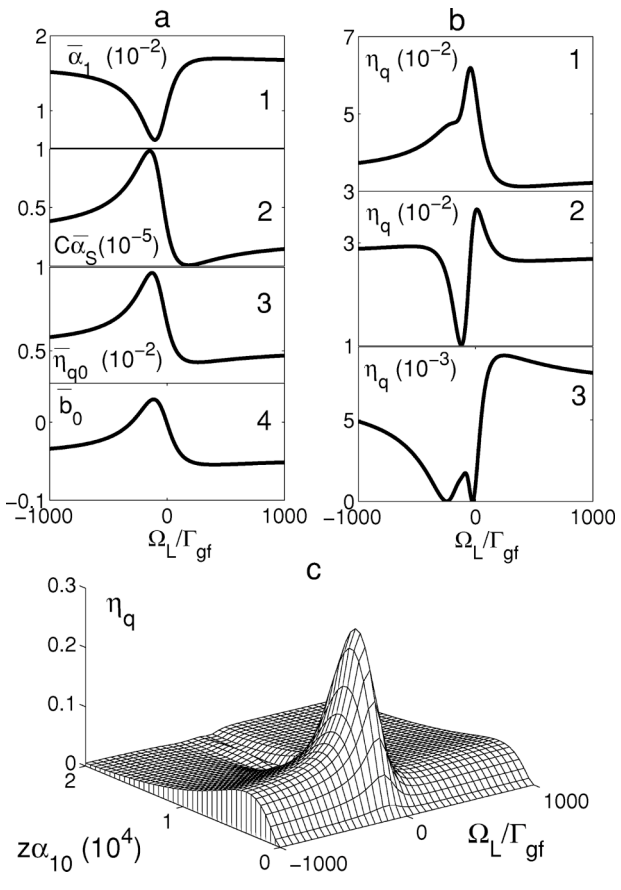

FIG. 7. Reduced absorption indices α_1/α_{10} and α_S/α_{10}; reduced squared modulus of the FWM polarization, $\bar{\eta}_{q0}$; and reduced difference of the conversion and absorption rates, $\bar{b}$ vs detuning Ω_L (a). Dependence of the quantum conversion efficiency η_q on Ω_L for $z\alpha_{10}=8.5\times10^3$ **(1)**, $z\alpha_{10}=1\times10^4$ **(2)**, and $z\alpha_{10}=2\times10^4$ **(3)** (b). Quantum conversion efficiency η_q vs optical thickness and Ω_L (c). Here, $C=10^{-5}$, $g_{ff}=150$, $g_{nn}=200$, $g_{mn}=9000$, $\Omega_1/\Gamma_{gf}=5000$, $\Omega_2/\Gamma_{gf}=-5100$, $q_{fg}=0.95$, $q_{gn}=-2$, $q_{ff}=0.01$, $q_{nn}=-5$, $q_{fn}=0$, $\Gamma_{gm}/\Gamma_{gf}=100$, $\Gamma_{gm}/\Gamma_{gn}=10$ (a–c).

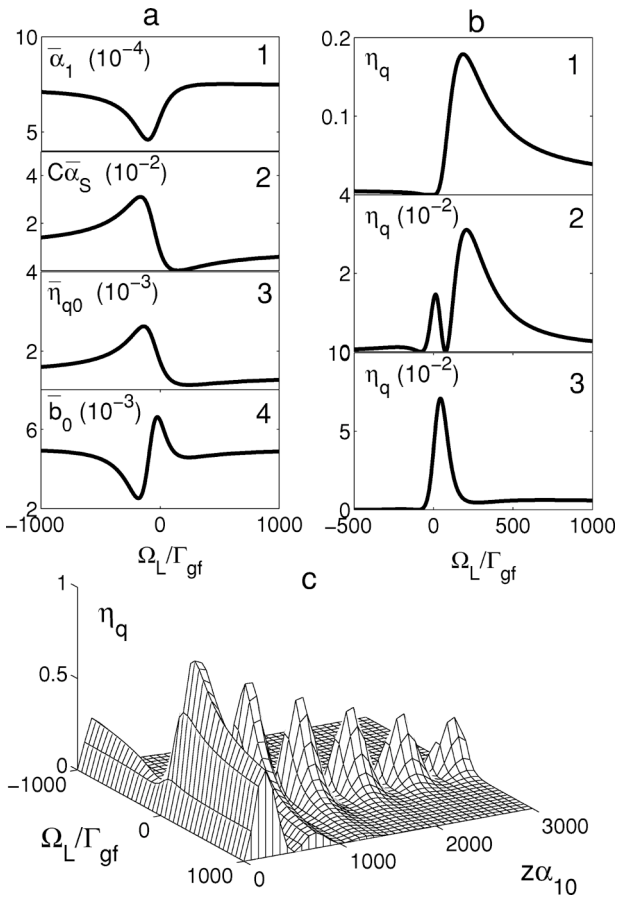

FIG. 8. Reduced absorption indices α_1/α_{10} and α_S/α_{10}; reduced squared modulus of FWM polarization, $\bar{\eta}_{q0}$; and reduced difference of conversion and absorption rates, $\bar{b}$ vs detuning Ω_L (a). Quantum conversion efficiency η_q vs Ω_L along the medium computed for $z\alpha_{10}=4.5\times10^2$ **(1)**, $z\alpha_{10}=5\times10^2$ **(2)**, and $z\alpha_{10}=5.5\times10^2$ **(3)** (b). Dependence of η_q on the optical thickness and on Ω_L (c). Here, $C=3\times10^{-2}$, $g_{nn}=500$, $g_{mn}=8000$ (a–c). The other parameters are the same as in Fig. 7.

the evolution of the generated radiation along the medium is substantially different and conversion is far from optimum [Figs. 7(b) and 7(c)].

Figure 8 is computed for the case where the detuning from a one-photon resonance is still large, but resonant absorption at the discrete transition and transition to the continuum differ less ($C=3\times10^{-2}$). In this case, the absorption coefficient α_1 can be decreased by a factor of 1.5, whereas the absorption coefficient α_S increases approximately threefold in one interval, but falls considerably in the other interval of Ω_L. Absorption at the transition into the continuum dominates practically throughout the whole range of the detuning $\Omega_L(\alpha_S/\alpha_1\approx70)$, and $\bar{\eta}_{q0}$ increases by a factor of 1.9 [Fig. 8(a)]. The quantity $\bar{b}$ is positive throughout the entire interval of Ω_L, having its maximum at a certain separation between two LICS. As that point, the conversion rate begins to exceed the rate of absorption so much that an oscillatory regime develops along the medium. The generation output from such a coherently prepared medium becomes strongly dependent on the optical density of the medium, i.e., on z or on the concentration N of atoms [Fig. 8(c)]. Thus the optimization of these values is required. At the first maximum (corresponding to $z\alpha_{10}\approx125$), the quantum conversion efficiency can reach 0.9 [Fig. 8(c)], which is *almost a complete quantum conversion of fundamental radiation to a short wavelength*, which efficiency is three times greater than in the preceding case. Since the energy of generated photons is several times greater than that of the fundamental ones, the power conversion efficiency may exceed several hundred percents, which is at the expense of energy of other driving fields. The dependence of the generated power on Ω_L along the medium also significantly changes [Fig. 8(b)] in regard to the absolute maximum, position and even the number of maxima (i.e., one maximum in plot 1 and two maxima in plot 2).

The above investigated regimes assume that one-photon frequency deviations are relatively large, and consequently a relatively high intensity of the fundamental radiations and/or optical density of the medium are required in order to achieve a maximum efficiency. The use of resonant processes makes it possible to reduce the required intensities

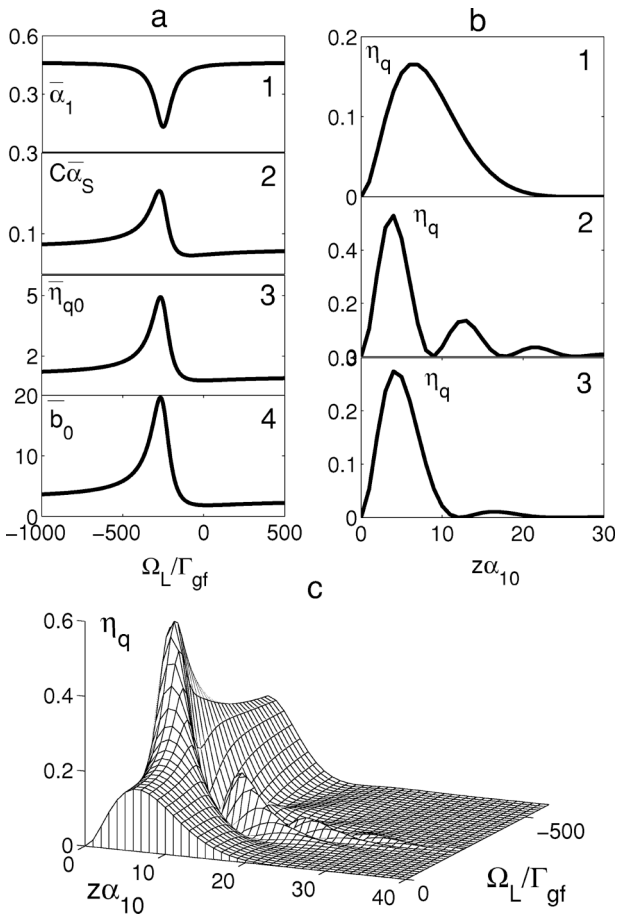

FIG. 9. Reduced absorption indices α_1/α_{10} and α_S/α_{10}; reduced squared modulus of FWM polarization, $\bar{\eta}_{q0}$; and reduced difference of conversion and absorption rates, $\bar{b}$ vs detuning Ω_L (a). Quantum conversion efficiency η_q vs optical thickness for $\Omega_L/\Gamma_{gf}=0$ **(1)**, $\Omega_L/\Gamma_{gf}=-250$ **(2)**, $\Omega_L/\Gamma_{gf}=-400$ **(3)** (b). Dependence of the quantum conversion efficiency η_q on the optical thickness and on Ω_L (c). Here, $g_{ff}=100$, $g_{nn}=5$, $g_{mn}=7$, $\Omega_1=0$, $\Omega_2/\Gamma_{gf}=-250$ (a–c). The other parameters are the same as in Fig. 8.

and to reach a fairly high conversion efficiency by optimization of the bleaching of the medium and enhancement of nonlinear-optical polarization through interference effects. Figure 9 illustrates such a case, where the ratio of the resonant absorption indices for discrete and continuous transitions is the same as in Fig. 8, but the coupling is entire resonance. The figure shows that at intensities of the radiation at ω_2, three orders of magnitude less than in the preceding case, it is possible to reduce the absorption index at ω_1 approximately by a factor of 10 compared with its value in the absence of strong fields. The maximum effect of the field E is a reduction in this index by a factor of 1.5 [Fig. 9(a)]. Here, the value of α_S increases approximately threefold, and $\bar{\eta}_{q0}$ by a factor of 4.7, and the absorption indices α_1 and α_S become comparable. Consequently, the nonlinear-optical conversion rate increases considerably over a fairly wide range of Ω_L, reaching a sharp maximum at $\Omega_L/\Gamma_{gf}=-250$. Depending on the spacing between two LICS, which control the interference, this may give rise to both a single maximum and to an oscillatory regime of generation along the medium [Figs. 9(b) and 9(c)]. This indicates the feasibility of total conversion of the radiations E_1 to E_S (and vice versa), apart from that lost by absorption, for some magnitude of products of the length of the medium and the number density of atoms. For the selected parameters, the conversion efficiency at the first maximum, where $z\alpha_{10}\approx 5$, reaches 0.54. This is less than in the preceding case, but such still high efficiency, where the power conversion may exceed 100%, is reached at much lower intensities and optical density of the medium.

The appropriate candidates for the realization of the proposed schemes are atoms among the II A and II B groups, which poses an energy-level spectrum that stretches into vacuum ultraviolet and is more equidistant compared to other elements. The characteristic field strength corresponding to values of $|G_{mn}|^2=(10\ldots1000)\Gamma_{gm}\Gamma_{gn}$ falls in the range of several parts of mW to several parts of W focused on the spot about several parts of mm. The characteristic intensity of the control field I, which is required to create a well-pronounced autoionizinglike resonance, is found from the equation $\gamma_{ff,nn}=\Gamma_{gf,gn}$. Assuming $\Gamma_{gf,gn}\approx 10^6-10^8\ s^{-1}$, photoionization cross section from the states f,n to equal $\sigma=10^{-17}$ cm^2, and $\hbar\omega=10^{-19}J$; from the equation $\gamma_{ff}=I\sigma/\hbar\omega$ one obtains: $I=(10^4-10^6)\mathrm{W/cm}^2$. Thus the required strength of the control field corresponds to the range of several parts of kW to several kW focused on the spot about several parts of mm. The resonance absorption length of about part of mm can be easily ensured from the ground state at partial vapor pressure of about one Torr. Hence the optical density of about 1000 corresponds to the cell lengths of about one cm. The continuous-wave regime implies the radiation pulse duration longer than characteristic relaxation time in the media. This corresponds to microsecond and longer pulses. It is assumed that ionizations do not substantially deplete the density of the resonant atoms which is ensured by the weakness of E_1 and consequently E_S fields. The other factor that works against the depletion is the exchange of atoms from inside and outside the beam, which at the thermal velocity about 5×10^2 m/s and the beam diameter 0.1 mm makes part of microsecond.

VII. CONCLUSIONS

A theory of nonlinear interference processes in a multilevel ladder-type quantum system is developed, which considers the coupling of several strong fields with adjacent bound-bound (discrete) and bound-free (continuous) transitions in the continuous wave regime, accounting for relaxation of coherence. The proposed scheme is an alternative to the approaches based on the concepts of coherent population trapping and maximum atomic coherence. The analytical solutions of coupled density-matrix equations is found and implemented for an analysis of the solution of Maxwell's equations describing four-wave mixing in a strongly absorbing medium. The theory is applied to the solution of two problems of practical importance.

The first problem concerns manipulating absorption and refractive indices both in the vicinity of discrete transitions and within the continuous short-wavelength spectra through the appropriate overlap of laser-induced continuous struc-

tures. Specific features attributed to quantum control in Doppler-broadened media, such as the formation of narrow sub-Doppler structures and the manipulation of transparency and dispersion by changing the relative propagation directions of the coupled waves, are shown. Thus, opportunities to create transparency and low dispersion, or alternatively, a large increase of these values within the narrow frequency bands of the required long-wavelength and short-wavelength intervals have been demonstrated through extensive numerical simulations based on typical possible atomic parameters. The applications may include frequency-tunable narrowband filters, polarization rotators, and dispersive elements for vacuum ultraviolet radiation.

Similar opportunities regarding manipulating the nonlinear four-wave mixing polarization of the medium have been studied as well. These were investigated in the context of the second problem, which is the large enhancement of short-wavelength generation and a decrease in the required intensities of the fundamental radiations by the use of fully resonant coupling and eradication of the negative effects of absorption through LICS-based coherent quantum control. Such opportunities become feasible through constructive and destructive interference of quantum pathways, which are different in lower-order and higher-order optical processes, and by the compensation of the nonlinear phase mismatch, which does not change along the media in the proposed scheme. Specific regimes of the generation along the absorptive media are analyzed, and discrimination factors for different types of behavior are found. A trade-off analysis of the accompanying nonlinear-interference processes in absorption as well as in four-wave mixing nonlinear polarization has been performed. The feasibility of the nearly complete conversion of low-frequency fundamental radiation to sum-frequency radiation is shown for the case of quasiresonant coupling. It is somewhat lower but still high for the case of fully resonant coupling which, however, requires a much less intense field. These feasibilities are based on quantum interference manipulated through an appropriate overlap of two LICS, which can be controlled by the strong field that does not contribute directly to four-wave mixing.

ACKNOWLEDGMENTS

This work has been supported in part by the International Association (INTAS) of the European Community (Grant No. INTAS-99-00019). The authors thank K. Bergmann for useful, encouraging discussions.

[1] G. E. Notkin, S. G. Rautian, and A. A. Feoktistov, Sov. Phys. JETP **25**, 1112 (1967).

[2] T. Ya. Popova, A. K. Popov, S. G. Rautian, and A. A. Feoktistov, Zh. Eksp. Teor. Fiz. **57**, 444 (1969) [Sov. Phys. JETP **30**, 243 (1970)] (http://xxx.lanl.gov/abs/quant-ph/0005081).

[3] T. Ya. Popova, A. K. Popov, S. G. Rautian, and R. I. Sokolovskii, Zh. Eksp. Teor. Fiz. **57**, 850 (1969) [Sov. Phys. JETP **30**, 466 (1970)] (http://xxx.lanl.gov/abs/quant-ph/0005094).

[4] M. S. Feld and A. Javan, Phys. Rev. **177**, 540 (1969); Th. Hansch, R. Keil, A. Schabert, Ch. Schmeltzer, and P. Toschek, Z. Phys. **226**, 293 (1969).

[5] S. G. Rautian and A. M. Shalagin, *Kinetic Problems of Nonlinear Spectroscopy* (North Holland, Amsterdam, 1991).

[6] A. K. Popov, *Introduction in Nonlinear Spectroscopy* (in Russian, Nauka, Novosibirsk, 1983).

[7] M. E. Movsesyan, N. N. Badalyan, and V. A. Iradyan, Pis'ma Zh. Eksp. Teor. Fiz. **6**, 631 (1967) [JETP Lett. **6**, 127 (1967)]; Yu. M. Kirin, D. P. Kovalev, S. G. Rautian, and R. I. Sokolovsky, *ibid.* **9**, 7 (1969) [*ibid.* **9**, 3 (1969)]; O. J. Lumpkin, Jr., IEEE J. Quantum Electron. **QE-4**, 226 (1968); M. P. Bondareva, Yu. M. Kirin, S. G. Rautian, V. P. Safonov, and B. M. Chernobrod, Opt. Spektrosk. **38**, 121 (1975) [Opt. Spectrosc. **38**, 121 (1975)].

[8] T. Ya. Popova, and A. K. Popov, Zh. Prikl. Spektrosk. **12** (989) 1970 [J. Appl. Spectrosc. **12**, 734 (1970)] (http://xxx.lanl.gov/abs/quant-ph/0005047); T. Ya. Popova and A. K. Popov, Izv. Vyssh. Uchebn. Zaved. Fiz. **11**, 38 (1970) [Sov. Phys. J. **13**, 1435 (1970)] (http://xxx.lanl.gov/abs/quant-ph/0005049).

[9] A. K. Popov and S. G. Rautian, in *Coherent Phenomena and Amplification without Inversion*, edited by A. V. Andreev, O. Kocharovskaya, and P. Mandel, Proc. SPIE **2798**, 49 (1996) (http://xxx.lanl.gov/abs/quant-ph/0005114); A. K. Popov, in *11th International Vavilov Conference on Nonlinear Optics*, edited by S. G. Rautian, Proc. SPIE **3485**, 252 (1998) (http://xxx.lanl.gov/abs/quant-ph/0005118).

[10] E. Arimondo, Prog. Opt. **35**, 259 (1996); S. E. Harris, Phys. Today **50**, 36 (1997).

[11] J. P. Marangos, J. Mod. Opt. **45**, 471 (1998).

[12] S. E. Harris, J. E. Field, and A. Imamoglu, Phys. Rev. Lett. **64**, 1107 (1990); M. Jain, H. Xia, G. Y. Yin, A. J. Merriam, and S. E. Harris, Phys. Rev. Lett. **77**, 4326 (1996); S. E. Harris, G. Y. Yin, M. Jain, H. Xia, and A. J. Merriam, Philos. Trans. R. Soc. London, Ser. A **355**, 2291 (1997); S. E. Harris and Y. Yamamoto, Phys. Rev. Lett. **81**, 3611 (1998); S. E. Harris and L. V. Hau, Phys. Rev. Lett. **82**, 4611 (1999).

[13] K. Hakuta, L. Marmet, and B. P. Stoicheff, Phys. Rev. Lett. **66**, 596 (1991); G. Z. Zhang, K. Hakuta, and B. P. Stoicheff, *ibid.* **71**, 3099 (1993).

[14] M. D. Lukin and A. Imamoglu, Phys. Rev. Lett. **84**, 1419 (2000); Nature (London) **413**, 237 (2001).

[15] Y. Wu, J. Saldana, and Y. Zhu, Phys. Rev. A **67**, 013811 (2003).

[16] L. Armstrong Jr., B. L. Beers, and S. Feneuille, Phys. Rev. A **12**, 1903 (1975).

[17] Yu. I. Heller and A. K. Popov, Opt. Commun. **18**, 7 (1976); Yu. I. Geller and A. K. Popov, Kvantovaya Elektron. (Moscow) **3**, 1129 (1976) [Sov. J. Quantum Electron. **6**, 606 (1976).

[18] Yu. I. Heller and A. K. Popov, Opt. Commun. **18**, 449 (1976).

[19] U. Fano, Phys. Rev. **124**, 1866 (1961); U. Fano and J. V.

Cooper, Rev. Mod. Phys. **40**, 441 (1968).

[20] Yu. I. Heller and A. K. Popov, Phys. Lett. **56A**, 453 (1976); Zh. Eksp. Teor. Fiz. **78**, 506 (1980) [Sov. Phys. JETP **51**, 255 (1980)].

[21] Yu. I. Heller and A. K. Popov, *Laser Induction of Nonlinear Resonanses in Continuous Spectra* (Novosibirsk, Nauka, 1981) [Engl. transl.: J. Sov. Laser Res. **6**, 1 (1985)].

[22] Yu. I. Geller, V. V. Lukinykh, A. K. Popov, and V. V. Slabko, Pis'ma Zh. Tekh. Fiz. **6**, 151 (1980) [Sov. Tech. Phys. Lett. **6**, 67 (1980)]; A. K. Popov, Yu. I Heller, V. F. Lukinykh, and V. V. Slabko, *Proceedings of the International Conference LASERS'80*, New Orleans (STS Press, McLean, VA, 1981), p. 735; Yu. I. Heller, V. F. Lukinykh, A. K. Popov, and V. V. Slabko, Phys. Lett. **82A**, 4 (1981); Yu. I. Geller, V. V. Lukinykh, A. K. Popov, and V. V. Slabko, Opt. Spektrosk. **51**, 732 (1981) [Opt. Spectrosc. **51**, 407 (1981)].

[23] Yu. I. Heller and A. K. Popov, Opt. Commun. **38**, 345 (1981); P. Lambropoulos and P. Zoller, Phys. Rev. A **24**, 379 (1981); K. Rzazewski and J. H. Eberly, Phys. Rev. Lett. **47**, 408 (1981); K. Rzazewski and J. H. Eberly, Phys. Rev. A **27**, 2026 (1983); P. L. Knight, M. A. Lauder, P. M. Radmore, and B. J. Dalton, Acta Phys. Austriaca **56**, 103 (1984); P. L. Knight, Comments At. Mol. Phys. **15**, 193 (1984); B.-N. Dai and P. Lambropoulos, Phys. Rev. A **36**, 5205 (1987); M. H. R. Hutchinson and K. M. M. Ness, Phys. Rev. Lett. **60**, 105 (1988); M. H. R. Hutchinson and K. M. M. Ness, Phys. Rev. Lett. **62**, 112 (1989); X. Tang, A. L'Huillier, and P. Lambropoulos, Phys. Rev. Lett. **62**, 111 (1989); P. L. Knight, M. A. Lander, and B. J. Dalton, Phys. Rep. **190**, 1 (1990); Y. L. Shao, D. Charalambidis, C. Fotakis, J. Zhang, and P. Lambropoulos, Phys. Rev. Lett. **67**, 3669 (1991); S. Cavalieri, F. S. Pavone, and M. Matera, Phys. Rev. Lett. **67**, 3673 (1991); O. Faucher, D. Charalambidis, C. Fotakis, J. Zhang, and P. Lambropoulos, Phys. Rev. Lett. **70**, 3004 (1993); S. Cavaliery, R. Eramo, and L. Fini, J. Phys. B **28**, 1739 (1995); S. Cavalieri, R. Eramo, R. Buffa, and M. Matera, Phys. Rev. A **51**, 2974 (1995); A. K. Popov, Bull. Russ. Acad. Sci. Phys. **60**, 927 (1996) (http://xxx.lanl.gov/abs/quant-ph/0005108); C. E. Carroll and F. T. Hioe, Phys. Rev. A **54**, 5147 (1996); A. D. Gazazyan and R. G. Unanyan, Laser Phys. **6**, 946 (1996); R. Eramo, S. Cavalieri, L. Fini, M. Matera, and L. F. DiMauro, J. Phys. B **30**, 3789 (1997); A. K. Popov and V. V. Kimberg, Kvantovaya Elektron. (Moscow) **25**, 236 (1998) [Quantum Electron. **28**, 228 (1998)]; O. Faucher, E. Hertz, B. Lavorel, R. Chaux, T. Dreier, H. Berger, and D. Charalambidis, J. Phys. B **32**, 4485 (1999).

[24] L. I. Pavlov, S. S. Dimov, D. I. Mechikov, G. M. Mileva, K. V. Stamenov, and G. B. Altschuler, Phys. Lett. **89A**, 441 (1982); S. S. Dimov, Yu. I. Heller, L. I. Pavlov, A. K. Popov, and K. V. Stamenov, Appl. Phys. B: Photophys. Laser Chem. **30**, 35 (1983); S. S. Dimov, Yu. I. Geller, L. I. Pavlov, and A. K. Popov, Kvantovaya Elektron. (Moscow) **10**, 1635 (1983) [Sov. J. Quantum Electron. **13**, 1075 (1983)]; O. Faucher, Y. L. Shao, and D. Charalambidis, J. Phys. B **26**, L309 (1993); O. Faucher, Y. L. Shao, D. Charalambidis, and C. Fotakis, Phys. Rev. A **50**, 641 (1994); A. K. Popov and V. V. Kimberg, Kvantovaya Elektron. (Moscow) **25**, 236 (1998) [Quantum Electron. **28**, 228 (1998)].

[25] T. Nakajima, M. Elk, J. Zhang, and P. Lambropoulos, Phys. Rev. A **50**, R913 (1994); E. Paspalakis, M. Protopapas, and P. L. Knight, Opt. Commun. **142**, 34 (1997); L. Yatsenko, R. Unanyan, K. Bergmann, T. Halfmann, and B. W. Shore, Opt. Commun. **135**, 406 (1997); E. Paspalakis, M. Protopapas, and P. L. Knight, J. Phys. B **31**, 775 (1998); R. G. Unanyan, N. V. Vitanov, and S. Stenholm, Phys. Rev. A **57**, 462 (1998); R. G. Unanyan, N. V. Vitanov, B. W. Shore, and K. Bergmann, Phys. Rev. A **61**, 043408 (2000).

[26] T. Halfmann, L. P. Yatsenko, M. Shapiro, B. W. Shore, and K. Bergmann, Phys. Rev. A **58**, R46 (1998); L. P. Yatsenko, T. Halfmann, B. W. Shore, and K. Bergmann, Phys. Rev. A **59**, 2926 (1999).

[27] N. P. Makarov, A. K. Popov, and V. P. Timofeev, Kvantovaya Elektron. (Moscow) **15**, 757 (1988) [Sov. J. Quantum Electron. **18**, 483 (1988)].

[28] A. K. Popov and V. M. Shalaev, Phys. Rev. A **59**, R946 (1999); A. K. Popov and A. S. Bayev, Phys. Rev. A **62**, 025801 (2000).